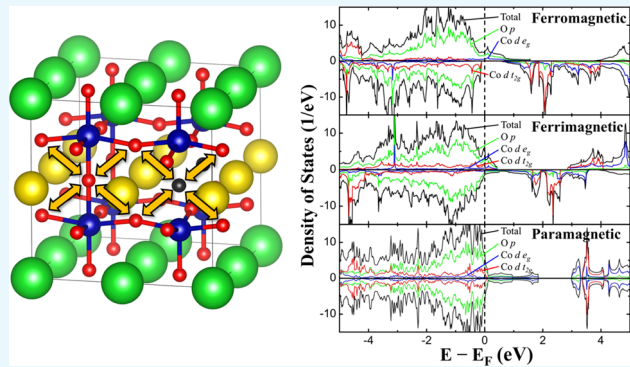


First-Principles Study of Anisotropic Oxygen Diffusion in $\text{PrBaCo}_2\text{O}_{5.5}$

Inseo Kim[†] and Minseok Choi^{*,†,‡}

[†]Department of Physics and [‡]Institute of Advanced Computational Science, Inha University, Incheon 22212, Republic of Korea

ABSTRACT: We address the anisotropic oxygen diffusion in $\text{PrBaCo}_2\text{O}_{5.5}$ using first-principles calculations based on the density functional theory. First, the experimentally observed magnetic properties such as ferromagnetic, ferrimagnetic, and paramagnetic phases are examined through systematic consideration of cobalt spin ordering and oxygen vacancy position. Then, the diffusion mechanism of an oxygen atom, assumed to be externally supplied, is explored by evaluating the oxygen migration barriers with the formation of one-dimensional oxygen-vacancy channel.



1. INTRODUCTION

Double perovskite $\text{RBaCo}_2\text{O}_{6-x}$ ($\text{R} = \text{Y}, \text{La-Ho}$: rare earth elements, $0 \leq x \leq 1$) has been investigated because of its various properties such as complicated magnetic structures, metal–insulator transition, and fast oxygen diffusion.^{1–9} Experiments have shown that cobalt 3d spin ordering and oxygen vacancy formation play a key role in the emergence of the properties, but understanding of their impact on the properties is still quite limited. Regarding $\text{PrBaCo}_2\text{O}_{5.5}$, a neutron and synchrotron experiment study¹⁰ observed cobalt ions at the center of the oxygen octahedra (Co_{Oct}) with the high spin (HS) state ($t_{2g}^4 e_g^2$, $S = 2$) and a spin transition to the low spin (LS) state ($t_{2g}^6 e_g^0$, $S = 0$) at high temperature, while cobalt spin state inside the oxygen pyramids (Co_{Py}) remains in the intermediate spin (IS) state ($t_{2g}^5 e_g^1$, $S = 1$). This leads to an antiferromagnetic-to-ferromagnetic transition at 215 K and a ferromagnetic-to-paramagnetic transition at 245 K. Zhang et al. also found such magnetic phase transitions at 145 and 195 K in $\text{PrBaCo}_2\text{O}_{5.5}$ and proposed the temperature-induced spin transition of cobalt from IS to HS.¹¹ Another neutron diffraction study reported the absence of ferromagnetic ordering and observed an antiferromagnetic-to-ferrimagnetic transition at 237 K and a ferrimagnetic-to-paramagnetic transition at 255 K.¹² This study suggests that the spin states of Co_{Oct} and Co_{Py} are, respectively, the mixed HS-IS and the mixed IS-LS states below 340 K; those acquire the IS state at higher temperature.

Above room temperature, an electronic transition, i.e., metal–insulator transition, occurs in $\text{PrBaCo}_2\text{O}_{5.5}$; this has been more consistently observed compared to above the magnetic transitions. The metal–insulator transition is found at 330–350 K, with a structural change from orthorhombic (space group $\text{Pmm}\alpha$) to another orthorhombic structure (space group Pmmm).^{10–13} Furthermore, the vacancy order-disorder

transition is measured at 776 K, leading to the transition from an orthorhombic to a tetragonal structure (space group $\text{P}4/\text{mmm}$), resulting from the rearrangement of oxygen vacancies.¹³

Owing to the fast oxygen diffusion, there is great interest in $\text{PrBaCo}_2\text{O}_{6-x}$ as promising cathode or electrolyte for the so-called intermediate-temperature solid-oxide fuel cells working in the temperature range of 500–700 °C.^{14–18} Although solid-oxide fuel cells have advantages such as high efficiency, fast reaction kinetics, fuel flexibility, and low emission of pollutants, their high operating temperature causes issues of degradation of cell materials, need for high-temperature-tolerant materials, and delay in start-up time.^{19,20} Therefore, huge efforts have been made recently to develop an intermediate-temperature solid-oxide fuel cells, and a comprehensive understanding of oxygen diffusion in the candidate oxide such as $\text{PrBaCo}_2\text{O}_{6-x}$ is of primary importance.

Experiments have consistently reported that oxygen atoms anisotropically diffuse through the oxide. An isotope-exchange depth profile study found anisotropic diffusion in $\text{PrBaCo}_2\text{O}_{5.5}$ with an activation energy of 1.02 eV by monitoring the differently oriented grains.²¹ The detailed pathway of diffusion in $\text{PrBaCo}_2\text{O}_{5.357}$ was described as an interlayer migration between the Pr–O and Co–O layers using the neutron diffraction method.²² Oxygen diffusion has also been investigated by computational approaches, but there are variations in the calculated results. A classical molecular dynamics study found anisotropic oxygen diffusion crossing the Pr–O and Co–O layers,²³ and similar result for oxygen vacancy migration was reported by first-principles calculation

Received: April 12, 2019

Accepted: June 11, 2019

Published: June 24, 2019

based on density functional theory,²⁴ although these provide much lower energy barriers for the migration (0.35²³ and 0.47 eV²⁴) in $\text{PrBaCo}_2\text{O}_{5.5}$. On the contrary, another computational work employing data-mining technique showed that the dominant diffusion would be given by the intralayer migration at the Co–O layers, having the lowest energy barrier in the calculations.²⁵

In the present study, our aim is to figure out the microscopic pathway of oxygen diffusion in $\text{PrBaCo}_2\text{O}_{5.5}$. We perform the first-principles density functional calculations with the Hubbard- U correction method. We first look at how cobalt spin ordering and oxygen vacancy influence the magnetic and electronic properties of $\text{PrBaCo}_2\text{O}_{5.5}$, and the experimental and theoretical observations in literatures are discussed for comparison. Oxygen diffusion is then investigated in terms of migration energy barrier based on convincing magnetic and crystal structures. One thing should be emphasized here is that our calculations consider one extra oxygen atom to elucidate more practical situation, which is the oxygen diffusion through the oxide in fuel cell devices. Previous computational studies have examined how the oxygen vacancy migrates, instead of oxygen atoms externally injected, by maintaining the chemical composition of the host oxides.^{21–25}

2. RESULTS AND DISCUSSION

Figure 1 shows the crystal structure of an orthorhombic $\text{PrBaCo}_2\text{O}_{5.5}$. The structure of $\text{PrBaCo}_2\text{O}_{5.5}$ is modeled by

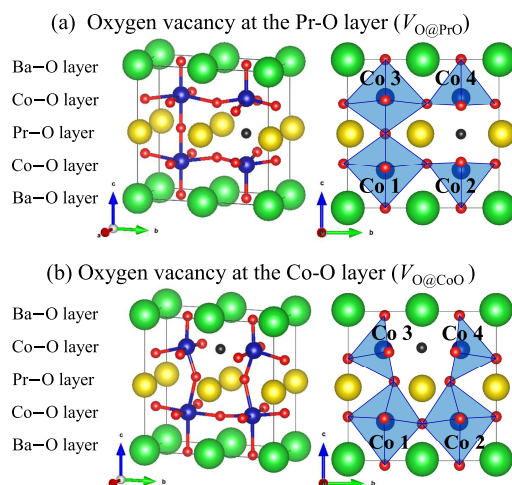


Figure 1. Unit cell structures of $\text{PrBaCo}_2\text{O}_{5.5}$, with one oxygen vacancy (gray) (a) at the Pr–O layer and (b) at the Co–O layer. Octahedral and pyramidal environment are formed by six and five nearest-neighbor oxygen ions (red), respectively.

doubling the mother material $\text{PrBaCo}_2\text{O}_6$ with an oxygen vacancy. Along the (001) crystal direction in the oxide, the Pr–O and the Ba–O atomic layers are alternately ordered, and the Co–O atomic layers are positioned between the Pr–O and the Ba–O layers. There are two types of cobalt ions, Co_{Oct} and Co_{Py} , in $\text{PrBaCo}_2\text{O}_{5.5}$ due to the presence of oxygen vacancy, while only Co_{Oct} exists in $\text{PrBaCo}_2\text{O}_6$.

Prior to examining the oxygen diffusion in $\text{PrBaCo}_2\text{O}_{5.5}$, magnetic configurations and the most likely position of oxygen vacancies should be investigated, since they determine the stable magnetic and crystal structures in which oxygen atoms diffuse. Again, we aim to address the diffusion of oxygen atom that is assumed to be externally injected. Experiments have

shown that oxygen vacancies are concentrated at the Pr–O layers, and our results also indicate that oxygen vacancy is most likely to form at the Pr–O layers ($V_{\text{O}@Pr\text{O}}$) compared to that at the Co–O layers ($V_{\text{O}@Co\text{O}}$) and at the Ba–O layers ($V_{\text{O}@Ba\text{O}}$) when the lattice parameters of the vacancy containing simulation cells were fully relaxed. For example, $V_{\text{O}@Pr\text{O}}$ is more stable than $V_{\text{O}@Co\text{O}}$ by 0.77 eV and $V_{\text{O}@Ba\text{O}}$ by 3.06 eV in the paramagnetic phase. Therefore, the lattice constant of the structure obtained with $V_{\text{O}@Pr\text{O}}$ is used even for the calculation of $V_{\text{O}@Co\text{O}}$ and $V_{\text{O}@Ba\text{O}}$. The calculated lattice constants for $V_{\text{O}@Pr\text{O}}$ are summarized for comparison with the experimental values in Table 1.

Table 1. Calculated Lattice Constants for Ferromagnetic, Ferrimagnetic, and Paramagnetic Phases, Having One Oxygen Vacancy at the Pr–O Layer^a

	ferromagnetic	ferrimagnetic	paramagnetic	experiment ⁵
<i>a</i> (Å)	3.966	3.965	3.907	3.908
<i>b</i> (Å)	3.997	4.008	4.043	3.937
<i>c</i> (Å)	7.813	7.798	7.812	7.611

^aExperimental values are included for comparison.

By taking into account several arrangements of Co 3d spins and oxygen vacancies, our calculations indicate that ferromagnetic, ferrimagnetic, and paramagnetic orderings are energetically likely to emerge in the oxide (Figure 2), and $V_{\text{O}@Pr\text{O}}$ is

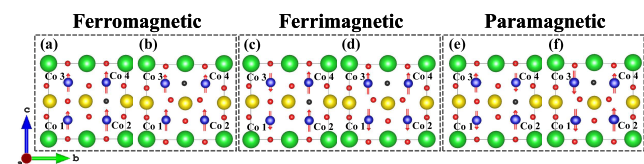


Figure 2. Possible configurations with the consideration of spin ordering and oxygen vacancy positions. (a, c, e) Oxygen vacancy formed at the Pr–O layer. (b, d, f) Oxygen vacancy formed at the Co–O layer.

more likely to form than $V_{\text{O}@Co\text{O}}$. The results explain the experimental^{5,6,10–13} and theoretical literatures^{23–25} reporting the concentrated oxygen vacancies at the Pr–O layers. $V_{\text{O}@Pr\text{O}}$ is more stable than $V_{\text{O}@Co\text{O}}$ by 1.05 eV in the ferromagnetic and by 0.71 eV in the ferrimagnetic phase. Structurally, the local atomic configuration around $V_{\text{O}@Pr\text{O}}$ is not remarkably changed, while it shows a strong distortion around $V_{\text{O}@Co\text{O}}$. We also find that the ferromagnetic spin ordering dramatically stabilizes the formation of $V_{\text{O}@Pr\text{O}}$ than does the paramagnetic ordering. $V_{\text{O}@Pr\text{O}}$ is more stable in the ferromagnetic phase than in the paramagnetic phase by 0.92 eV. On the other hand, $V_{\text{O}@Pr\text{O}}$ shows similar stability both in the ferromagnetic and ferrimagnetic phases. The energy difference of $V_{\text{O}@Pr\text{O}}$ between the two phases is calculated to be only 0.01 eV. Such a small difference seems to explain the controversial experimental observation of ferromagnetic and ferrimagnetic phases.^{10–12} Regarding $V_{\text{O}@Co\text{O}}$, the vacancy in the ferromagnetic phase is less stable than that in the ferrimagnetic phase by 0.33 eV, differing from the $V_{\text{O}@Pr\text{O}}$ case. $V_{\text{O}@Ba\text{O}}$ is quite unlikely to form in the oxide compared to $V_{\text{O}@Pr\text{O}}$. $V_{\text{O}@Ba\text{O}}$ is found to be less stable than $V_{\text{O}@Pr\text{O}}$ by 1.84 eV in the ferromagnetic phase, by 1.93 eV in the ferromagnetic phase, and by 3.10 eV in the paramagnetic phase.

Moving to electronic property, the calculated density of states for $V_{O@PrO}$ in $\text{PrBaCo}_2\text{O}_{5.5}$ are shown in Figure 3.

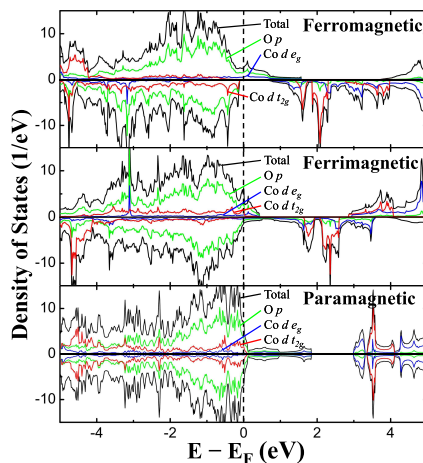


Figure 3. Density of states for three magnetic phases having one oxygen vacancy at the Pr–O layer. The Fermi level is set as zero.

$\text{PrBaCo}_2\text{O}_{5.5}$ exhibits a metallic feature irrespective of the magnetic ordering, and the states at the Fermi level are characterized by the Co 3d–O 2p hybridization. Co_{Oct} and Co_{Py} possess, respectively, 2.60 and $2.21 \mu_B$ in the paramagnetic-metal phase, which correspond to the IS states with slightly larger values than the ideal value ($2 \mu_B$) for the IS state. This is consistent with the experimental suggestion by Miao et al.¹² but differs from other suggestions that explain the metal–insulator transition.^{10,11} In the ferromagnetic phase, Co_{Oct} has $2.63 \mu_B$ and Co_{Py} does $3.10 \mu_B$, and they have the same values in the ferrimagnetic phase.

It is noteworthy that our results do not agree with the experimental finding of the electronic properties; in addition, the paramagnetic–insulator phase could not be reproduced in the calculations. Ferromagnetic and ferrimagnetic phases are experimentally known to be insulating, and paramagnetic phase is also insulating below room temperature and becomes metallic at higher temperature in conjunction with a structural symmetry change from $Pmnma$ to $Pmmm$. In fact, one previous density functional study also reported that $\text{PrBaCo}_2\text{O}_{5.5}$ is metallic.²⁴ Thus, it cannot be excluded that the discrepancy may arise from the limit of computational approach in the present work. However, our main aim is to address the oxygen diffusion in $\text{PrBaCo}_2\text{O}_{5.5}$, and we believe our computational approach provides a better understanding of the microscopic mechanism of oxygen diffusion in the oxide. In practice, the following results in the present work explain well the experimental observations.

Finally, we attempt to address oxygen diffusion in terms of migration barriers. The paramagnetic phase is chosen for the calculations, since it may correspond to the temperature range of interest for the intermediated temperature fuel cell application. Our calculations are carried out based on the following reasoning. To practically simulate the oxygen diffusion process in the case that $\text{PrBaCo}_2\text{O}_{5.5}$ is implemented in the fuel cell device, one added oxygen atom is assumed to be externally supplied as a fuel. When an oxygen atom comes into the oxide, at the beginning, the oxygen may prefer to occupy one of the oxygen vacancies or to be positioned near the vacant sites in the one-dimensional vacancy channel-like structure formed at the Pr–O layers. In case of the former, the possible

path of oxygen migration to the next position would be six by crystal symmetry, as illustrated in Figure 4. The migration

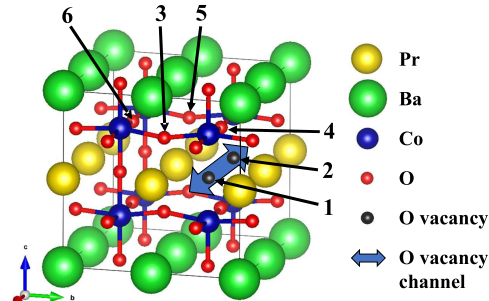


Figure 4. Six migration paths for oxygen atom. Black solid circle denotes the oxygen vacancies, and blue arrow indicates the one-dimensional oxygen vacancy channel along the a -axis. Several sites of oxygen ion, corresponding to paths 1–6, are pointed as a number.

energy barriers for the six paths thus determine the most likely diffusion path in terms of energy. It is also expected that the position of oxygen in the latter case may appear to be the lowest energy point between the calculated migration path. We exclude the Ba–O layers in which the formation of oxygen vacancy is highly unlikely, as we discussed above.

As shown in Figure 4, the oxygen ion site 1–2 represent the oxygen migration along the channel in the Pr–O layers (path 1). Sites 1–3 and 1–4 correspond to the migration from the Pr–O layer to the Co–O layer (paths 2 and 3, respectively). Sites 3–4, 3–5, and 4–6 are responsible for the oxygen migration in the Co–O layers (paths 4–6, respectively). The calculated energy barriers are summarized in Table 2. The

Table 2. Calculated Migration Barriers for Paths 1–6

	path	sites	migration barrier (eV)
Intra Pr–O layer	1	1 → 2	1.27
Pr–O to Co–O layer or vice versa	2	1 → 3	0.99
	3	1 → 4	1.79
Intra Co–O layer	4	3 → 4	1.20
	5	3 → 5	1.69
	6	4 → 6	2.72

oxygen diffusion path is found to be highly anisotropic and have a two-dimensional network, possibly moving in a zigzag manner. Oxygen atom migration along path 2 is energetically favorable, and the calculated energy barrier is 0.99 eV , which is close to the experimental values of 1.02 eV obtained using the isotope exchange depth profile method²¹ and 1.20 eV extracted using the Arrhenius plot based on the area specific resistance.²⁶ The results lead us to conclude that when an oxygen atom comes into the oxide, it favors to move across the atomic layers along the (011) (and symmetrically identical) direction, which is perpendicular to the one-dimensional oxygen-vacancy channel. This explains a neutron diffraction study reporting the alternate movement of oxygen from the Pr–O to Co–O layers or vice versa in the tetragonal $\text{PrBaCo}_2\text{O}_{5.5}$.²² Similar anisotropic pathways for vacancy migration in $\text{PrBaCo}_2\text{O}_{5.5}$ was suggested with lower-energy barriers by the previous theoretical studies, although these studies do not examine an externally injected oxygen atom like in the present work but the oxygen vacancy. A classical molecular dynamics simulation

reports anisotropic vacancy migration with an energy barrier of 0.35 eV in the temperature range from 650 to 1000 °C.²³ An earlier density functional study also suggests that oxygen migration between the Pr–O and Co–O layers is favorable in ferromagnetic (and metallic) orthorhombic $\text{PrBaCo}_2\text{O}_{5.5}$, and the energy barrier for migration is calculated to be 0.47 eV.²⁴

However, another molecular dynamics simulation with data mining proposes that oxygen migration is constrained to the Co–O layers in $\text{PrBaCo}_2\text{O}_{5.5}$ with the barrier of 0.27 eV.²⁵ According to our results, a much higher migration barrier (1.20 eV) should be overcome for migration to the Co–O layers, and it seems that the discrepancy comes from the missing quantum mechanical description of a strong Co–O chemical bonding and dealing with high temperature up to 1573 K in ref 25.

3. CONCLUSIONS

We have carried out first-principle calculations to investigate the oxygen diffusion in double perovskite $\text{PrBaCo}_2\text{O}_{5.5}$. Ferromagnetic, ferrimagnetic, and paramagnetic phases, which were experimentally reported, were found with one oxygen vacancy. All of the magnetic phases were electronically metallic, and the state of the Fermi level exhibits the mixed oxygen 2p and cobalt 3d characterization. Surprisingly, cobalt ions in both octahedral and pyramidal sites possess an intermediate spin state in the paramagnetic phase, differing from the typical interpretation of the metal–insulator transition in $\text{PrBaCo}_2\text{O}_{6-x}$. Oxygen diffusion path was examined on the basis of the obtained magnetic and vacant structures. The paramagnetic orthorhombic phase was taken into account for the diffusion calculations, since it is responsible for the situation in the temperature range of interest for intermediate temperature solid-oxide fuel cell applications. We conclude that the main contribution of oxygen diffusivity is attributed to the migration from the Pr–O layer to the Co–O layer or vice versa along the direction perpendicular to the one-dimensional oxygen-vacancy channel.

4. COMPUTATIONAL DETAILS

Our calculations were performed using the project-augmented wave method²⁷ and the generalized gradient approximation in the Perdew–Burke–Ernzerhof scheme,²⁸ with the Hubbard-U correction as implemented in the Vienna ab initio simulation package code.²⁹ A rotationally invariant +U method was applied for the Co 3d states. In general, the U-values are taken from the literature or are selected in a specific way such as to calibrate the values, which reproduce the experimentally measured magnetic moments in the given system.³⁰ Here, we considered the former and the effective U-value (U_{eff}) of 5.0 eV, which provides reliable results in the related materials.^{31,32} The electronic wave functions were expanded in a plane wave basis set with an energy cutoff of 400 eV. The calculations were performed using $\text{PrBaCo}_2\text{O}_{5.5}$ unit cells containing 19 atoms with one oxygen vacancy. The integrations over the Brillouin zone were carried out using an $8 \times 8 \times 4$ k-point grid. All of the lattice parameters and atomic coordinates were fully optimized until the Hellmann–Feynman forces were less than 0.02 eV/Å. For simulating oxygen ion diffusion, $2 \times 2 \times 1$ supercells containing 40 atoms and a $4 \times 4 \times 4$ k-point grid were used.

We specified initial magnetic moments for each Co atom considering the crystal field effect at the Co sites (octahedral

and pyramidal symmetry). In the calculations, the Pr 4f orbitals were treated as the core states (valence electron configuration: $5s^25p^65d^16s^2$) in the Pr pseudopotential, since Pr is not attributed to the experimentally observed magnetization above the temperature of 20 K,^{10,12,33} and the treatment of Pr 4f as the valence states in the pseudopotential is known to have nonphysical computational consequences.^{34,35}

■ AUTHOR INFORMATION

Corresponding Author

*E-mail: minseok.choi@inha.ac.kr. Phone: +82-32-860-7656. Fax: +82-32-872-7562.

ORCID

Minseok Choi: 0000-0001-8967-3030

Author Contributions

The manuscript was written through contributions of all authors. All authors have given approval to the final version of the manuscript.

Notes

The authors declare no competing financial interest.

■ ACKNOWLEDGMENTS

The authors thank Professor Hyunjeen Jeon for useful discussion and comments. This work was supported by Inha University Research Grant (INHA-58357).

■ REFERENCES

- (1) Roy, S.; Dubenko, I. S.; Khan, M.; Condon, E. M.; Craig, J.; Ali, N.; et al. Magnetic Properties of Perovskite-Derived Air-Synthesized $\text{RBaCo}_2\text{O}_{5+\delta}$ ($R = \text{La}–\text{Ho}$) Compounds. *Phys. Rev. B* **2005**, *71*, No. 024419.
- (2) Conder, K.; Pomjakushina, E.; Pomjakushin, V.; Stingaci, M.; Streule, S.; Podlesnyak, A. Oxygen Isotope Effect on Metal–Insulator Transition in Layered Cobaltites $\text{RBaCo}_2\text{O}_{5.5}$ ($R = \text{Pr}, \text{Dy}, \text{Ho}$ and Y). *J. Phys.: Condens. Matter* **2005**, *17*, 5813–5820.
- (3) Makhnev, A. A.; Nomerovannaya, L. V.; Strel'tsov, S. V.; Anisimov, V. I.; Barilo, S. N.; Shiryaev, S. V. Metal–Insulator Transition in Double Cobaltites $\text{RBaCo}_2\text{O}_{5.5}$ ($R = \text{Eu}, \text{Gd}$): Specific Features of Their Optical Properties. *Phys. Solid State* **2009**, *51*, 525–531.
- (4) Luetkens, H.; Stingaci, M.; Pashkevich, Y. G.; Conder, K.; Pomjakushina, E.; Gusev, A. A.; Lamanova, K. V.; Lemmens, P.; Klauss, H.-H. Microscopic Evidence of Spin State Order and Spin State Phase Separation in Layered Cobaltites $\text{RBaCo}_2\text{O}_{5.5}$ with $R = \text{Y}, \text{Tb}, \text{Dy}$, and Ho . *Phys. Rev. Lett.* **2008**, *101*, No. 017601.
- (5) Rautama, E. L.; Karppinen, M. R-Site Varied Series of $\text{RBaCo}_2\text{O}_{5.5}$ ($R_2\text{Ba}_2\text{Co}_4\text{O}_{11}$) Compounds with Precisely Controlled Oxygen Content. *J. Solid State Chem.* **2010**, *183*, 1102–1107.
- (6) Maignan, A.; Martin, C.; Pelloquin, D.; Nguyen, N.; Raveau, B. Structural and Magnetic Studies of Ordered Oxygen-Deficient Perovskites $\text{LnBaCo}_2\text{O}_{5+\delta}$ Closely Related to the “112” Structure. *J. Solid State Chem.* **1999**, *142*, 247–260.
- (7) Moritomo, Y.; Akimoto, T.; Takeo, M.; Machida, A.; Nishibori, E.; Takata, M.; Sakata, M.; Ohoyama, K.; Nakamura, A. Metal–Insulator Transition Induced by a Spin-State Transition in $\text{TbBaCo}_2\text{O}_{5+\delta}$ ($\delta = 0.5$). *Phys. Rev. B* **2000**, *61*, No. R13325.
- (8) Frontera, C.; García-Muñoz, J. L.; Llobet, A.; Aranda, M. A. G. Selective Spin-State Switch and Metal–Insulator Transition in $\text{GdBaCo}_2\text{O}_{5.5}$. *Phys. Rev. B* **2002**, *65*, No. 180405.
- (9) Wu, H. High Spin, Hole Delocalization and Electron Transfer in $\text{LBaCo}_2\text{O}_{5.5}$ ($L = \text{Sm}, \text{Eu}, \text{Gd}, \text{Tb}, \text{Dy}, \text{Y}$). *J. Phys.: Condens. Matter* **2003**, *15*, S03.
- (10) Frontera, C.; García-Muñoz, J.; Carrillo, A. E.; Aranda, M. A. G.; Margiolaki, I.; Caneiro, A. Spin State of Co^{3+} and Magnetic

- Transitions in $\text{RBaCo}_2\text{O}_{5.50}$ ($R = \text{Pr, Gd}$): Dependence on Rare-Earth Size. *Phys. Rev. B* **2006**, *74*, No. 054406.
- (11) Zhang, X.; Wang, X. M.; Wei, H. W.; Lin, X. H.; Wang, C. H.; Zhang, Y.; Chen, C.; Jing, X. P. Effect of Oxygen Content on Transport and Magnetic Properties of $\text{PrBaCo}_2\text{O}_{5.50+\delta}$. *Mater. Res. Bull.* **2015**, *65*, 80–88.
- (12) Miao, P.; Lin, X.; Lee, S.; Ishikawa, Y.; Torii, S.; Yonemura, M.; Ueno, T.; Inami, N.; Ono, K.; Wang, Y.; Kamiyama, T. Hole-Doping-Induced Melting of Spin-State Ordering in $\text{PrBaCo}_2\text{O}_{5.5+x}$. *Phys. Rev. B* **2017**, *95*, No. 125123.
- (13) Streule, S.; Podlesnyak, A.; Sheptyakov, D.; Pomjakushina, E.; Stingaci, M.; Conder, K.; Medarde, M.; Patrakeev, M. V.; Leonidov, I. A.; Kozhevnikov, V. L.; Mesot, J. High-Temperature Order-Disorder Transition and Polaronic Conductivity in $\text{PrBaCo}_2\text{O}_{5.48}$. *Phys. Rev. B* **2006**, *73*, No. 094203.
- (14) Wang, W.; Peh, T. S.; Chan, S. H.; Zhang, T. S. Synthesis and Characterization of $\text{LnBaCo}_2\text{O}_{5+\delta}$ Layered Perovskites as Cathodes for Intermediate-Temperature Solid Oxide Fuel Cells. *ECS Trans.* **2009**, *25*, 2277–2281.
- (15) Zhao, L.; He, B.; Lin, B.; Ding, H.; Wang, S.; Ling, Y.; Peng, R.; Meng, G.; Liu, X. High Performance of Proton-Conducting Solid Oxide Fuel Cell with a Layered $\text{PrBaCo}_2\text{O}_{5+\delta}$ Cathode. *J. Power Sources* **2009**, *194*, 835–837.
- (16) Liu, J.; Collins, G.; Liu, M.; Chen, C.; He, J.; Jiang, J.; Meletis, E. I. Ultrafast Oxygen Exchange Kinetics on Highly Epitaxial $\text{PrBaCo}_2\text{O}_{5+\delta}$ Thin Films. *Appl. Phys. Lett.* **2012**, *100*, No. 193903.
- (17) Gao, Y.; Chen, D.; Chen, C.; Shao, Z.; Ciucci, F. Oriented $\text{PrBaCo}_2\text{O}_{5+\delta}$ Thin Films for Solid Oxide Fuel Cells. *J. Power Sources* **2015**, *278*, 623–629.
- (18) Enriquez, E.; Xu, X.; Bao, S.; Harrell, Z.; Chen, C.; et al. Catalytic Dynamics and Oxygen Diffusion in Doped $\text{PrBaCo}_2\text{O}_{5.5+\delta}$ Thin Films. *ACS Appl. Mater. Interfaces* **2015**, *7*, 24353–24359.
- (19) Steele, B. C. H.; Heinzel, A. Materials for Fuel-Cell Technologies. *Nature* **2001**, *414*, 345–352.
- (20) Brett, D. J. L.; Atkinson, A.; Brandon, N. P.; Skinner, S. J. Intermediate Temperature Solid Oxide Fuel Cells. *Chem. Soc. Rev.* **2008**, *37*, 1568–1578.
- (21) Burriel, M.; Peña-Martínez, J.; Chater, R. J.; Fearn, S.; Berenov, A. V.; Skinner, S. J.; Kilner, J. A. Anisotropic Oxygen Ion Diffusion in Layered $\text{PrBaCo}_2\text{O}_{5+\delta}$. *Chem. Mater.* **2012**, *24*, 613–621.
- (22) Chen, Y. C.; Yashima, M.; Peña-Martínez, J.; Kilner, J. A. Experimental Visualization of the Diffusional Pathway of Oxide Ions in a Layered Perovskite-Type Cobaltite $\text{PrBaCo}_2\text{O}_{5+\delta}$. *Chem. Mater.* **2013**, *25*, 2638–2641.
- (23) Seymour, I. D.; Tarancón, A.; Chroneos, A.; Parfitt, D.; Kilner, J. A.; Grimes, R. W. Anisotropic Oxygen diffusion in $\text{PrBaCo}_2\text{O}_{5.5}$ Double Perovskite. *Solid State Ion.* **2012**, *216*, 41–43.
- (24) Akande, S. O.; Boulfrad, S.; Schwingenschlögl, U. Intrinsic Defect Processes and O Migration in $\text{PrBa}(\text{Co/Fe})_2\text{O}_{5.5}$. *J. Mater. Chem. A* **2016**, *4*, 3560–3564.
- (25) Chen, C.; Chen, D.; Ciucci, F. A Molecular Dynamics Study of Oxygen Ion Diffusion in A-Site Ordered Perovskite $\text{PrBaCo}_2\text{O}_{5.5}$: Data Mining the Oxygen Trajectories. *Phys. Chem. Chem. Phys.* **2015**, *17*, 7831–7837.
- (26) Jiang, X.; Shi, Y.; Zhou, W.; Li, X.; Su, Z.; Pang, S.; Jiang, L. Effects of Pr^{3+} -Deficiency on Structure and Properties of $\text{PrBaCo}_2\text{O}_{5+\delta}$ Cathode Material—A Comparison with Ba^{2+} -Deficiency Case. *J. Power Sources* **2014**, *272*, 371–377.
- (27) Blöchl, P. E. Projector Augmented-Wave Method. *Phys. Rev. B* **1994**, *50*, No. 17953.
- (28) Perdew, J. P.; Burke, K.; Ernzerhof, M. Generalized Gradient Approximation Made Simple. *Phys. Rev. Lett.* **1996**, *77*, No. 3865.
- (29) Kresse, G.; Hafner, J. *Ab initio* Molecular for Liquid Metals. *Phys. Rev. B* **1993**, *47*, No. 558.
- (30) Das, T.; Nicholas, J. D.; Yue, Q. Long-range charge transfer and oxygen vacancy interactions in strontium ferrite. *J. Mater. Chem. A* **2017**, *5*, 4493.
- (31) Wu, H. Spin State and Phase Competition in $\text{TbBaCo}_2\text{O}_{5.5}$ and the Lanthanide Series $\text{LBaCo}_2\text{O}_{5+\delta}$ ($0 \leq \delta \leq 1$). *Phys. Rev. B* **2001**, *64*, No. 092413.
- (32) Maria, J.; Nazir, S.; Alay-e-Abbas, S. M.; Shaukat, A. Half-Metallic Ferromagnetism in Ordered $\text{LaBaCo}_2\text{O}_6$ and Disordered $\text{La}_{0.5}\text{Ba}_{0.5}\text{CoO}_3$: DFT + U Study. *J. Magn. Magn. Mater.* **2014**, *368*, 230–233.
- (33) Li, W. H.; Chang, K. J.; Hsieh, W. T.; Lee, K. C.; Lynn, J. W.; Yang, H. D. Magnetic Ordering of Pr in $\text{PrBa}_2\text{Cu}_{2.7}\text{Zn}_{0.3}\text{O}_{7-y}$. *Phys. Rev. B* **1993**, *48*, No. 519.
- (34) Zhao, H. J.; Ren, W.; Yang, Y.; Íñiguez, J.; Chen, X. M.; Bellaiche, L. Near Room-Temperature Multiferroic Materials with Tunable Ferromagnetic and Electrical Properties. *Nat. Commun.* **2014**, *5*, No. 4021.
- (35) Topsakal, M.; Leighton, C.; Wentzcovich, R. M. First-Principles Study of Crystal and Electronic Structure of Rare-Earth Cobaltites. *J. Appl. Phys.* **2016**, *119*, No. 244310.